Effects of Al and refractory alloying elements (W, Ta and Hf) on oxidation kinetics, oxygen dissolution and diffusion in titanium alloys

Kevin Gautier, Enrica Epifano, Thomas Gheno, Damien Connétable, Daniel Monceau

Effects of Al and refractory alloying elements (W, Ta and Hf) on oxidation kinetics, oxygen dissolution and diffusion in titanium alloys

Kevin Gautier[1], Enrica Epifano[1], Thomas Gheno[2], Damien Connétable[1], Daniel Monceau[1]

1: CIRIMAT, Université de Toulouse, CNRS, INPT, UPS, 4 allée Emile Monso, BP 44362, 31030 Toulouse Cedex 4, France
2: DMAS, ONERA, Université Paris-Saclay, 92322 Châtillon, France

Abstract:

The effect of aluminium, tungsten, tantalum and hafnium on the oxidation behaviour of titanium was investigated. Model alloys were oxidized in air for 5000 h at 650 °C. All alloying elements decreased oxide growth and oxygen dissolution in the metal; tungsten was the most efficient. The oxygen diffusivity decreased with aluminium. Tungsten enhanced the formation of Ti_2N at the oxide/metal interface which decreased oxygen dissolution in the alloys. Experiments in Ar-20%O_2, where Ti_2N could not form, confirmed the major role of nitrogen on the oxidation resistance of tungsten-containing alloys. The ternary model alloy Ti-10Al-2W outperformed the high-temperature alloy Ti6242S.

Keywords: Titanium-based alloys, high temperature oxidation, refractory element, tungsten, oxygen dissolution

Introduction

The aerospace industry has been working for decades to reduce the carbon footprint of air transport by decreasing aircraft weights. Titanium-based alloys are now widely used in structural parts due to their low density [1]. However, nickel-based alloys or steels are still used in the hottest parts of aircraft engines because of their better oxidation and creep resistance. One of the proposals to lighten aircraft is to replace some of these heavy alloys with titanium alloys, which can have better specific mechanical properties. Nevertheless, for now, the use of titanium alloys is limited to temperatures below 550 °C due to insufficient oxidation [2] and creep resistance [3] at higher temperatures.

The oxidation of titanium alloys involves two main processes: the formation of an oxide scale, mainly composed of rutile TiO_2, and the important diffusion of oxygen into the alloy, due to the high solubility of oxygen in the alloy, which is up to 33 at. % for pure α-Ti [4]. The second phenomenon is the most detrimental: it leads to the formation of an oxygen-affected zone (OAZ), which is very brittle and about 5 to 10 times thicker than the oxide layer [5]. This phenomenon is also referred to as “oxygen embrittlement”. Previous studies have shown that the brittle-to-ductile transition induced by oxygen occurs for concentrations as low as below 1 at. % in Ti64

(Ti-6 wt. % Al-4 wt. % V) [6], and 0.5 at. % in Ti6242S [7] at room temperature. In order to increase the service temperature of titanium alloys, it is necessary to limit the oxygen intake in the alloy. One possibility to achieve this is to decrease the oxygen solubility and/or the diffusivity through alloying. Decreasing the solubility, i.e. the oxygen concentration under the oxide scale, or decreasing the diffusion coefficient of oxygen in the metal will both result in a thinner OAZ.

Many studies were conducted on the effect of alloying elements on oxidation kinetics and oxygen diffusion of titanium alloys in air. Chaze et al. studied the influence of Al between 550 °C and 700 °C [8, 9]. They showed that increasing the Al content causes a decrease of the oxidation kinetics in both air and pure oxygen atmospheres, with a small decrease in the O diffusivity at 700 °C. Other elements are known to limit the oxidation rate, such as Si [10-12] and Nb [13, 14]. Ramoul et al. showed the detrimental effect of V on oxidation kinetics [15], which explains the low oxidation resistance of Ti64 for temperatures above 550 °C. Adding Sn also increases oxidation rates [16].

Huvelin et al. showed that refractory elements can improve creep resistance at 600 °C [17]. There are some studies based on the effect of refractory elements on oxidation kinetics. Hanrahan et al. [18-20] showed a decrease in oxidation rate in the presence of Ta between 800 °C and 1400 °C, but at very high concentration (up to 40 wt. % Ta), and at temperatures not suitable for many applications because of very high oxidation rates at these temperatures. Xu et al. showed an increase in oxidation resistance by adding W in Ti-6.5Al-2Sn-4Hf-2Nb alloy in air at 750 °C [21]. Kitashima et al. studied binaries alloys by adding 0.38 wt. % W, 13.45 wt. % Hf, 7.36 wt. % Zr and 0.05 wt. % Si, and showed a decrease in oxidation rates in the presence of these elements, by comparison with pure titanium [22]. Finally, Maynor and Swift studied many binary and ternary alloys and concluded that ternary Ti-Ta-Si, Ti-W-Si and Ti-Al-Si had the lowest oxidation rate between 650 °C and 980 °C [23]. Of course, for an aeronautical application, the addition of heavy refractory elements is not obvious. It must be demonstrated that the gain in creep resistance compensates the increase in mass. Il must also be shown that these elements improve or at least do not degrade the oxidation resistance.

None of these studies investigated the effect of these alloying elements on oxygen diffusivity and solubility, the two main quantities that influence the depth of the OAZ. In this study, both the overall oxidation kinetics and the oxygen diffusivity were determined in air and in Ar-20%O_2 in binary and ternary alloys containing Al, Ta, W or Hf, by discontinuous weighing, X-Ray Diffraction (XRD), Scanning Electron Microscopy (SEM) observations and Electron Probe Micro-Analysis (EPMA) measurements.

Experimental procedures

Materials

Titanium alloys were fabricated as 40-50 g ingots by arc melting in a ECM Technologies electric arc furnace, from grade 2 titanium and better than 99.95 % pure Al, Ta, W, Hf (Ti and Ta were obtained from Acal BFi, Al from Pechiney, W and Hf from Neyco). The raw materials were provided as rods (2 to 6 mm diameter), except W which was provided as a 44 µm-diameter powder, and enveloped in an Al sheet (in Al-containing alloys) or in a Ti sheet. Before starting the arc, the furnace chamber was placed under a 10^{-6} mbar vacuum and then filled with 300 mbar Ar. The ingots were remelted 10-15 times to ensure chemical homogeneity. After elaboration, the major element concentrations were measured by inductively coupled plasma-optical emission spectroscopy (Spectro Ciros), and O and N concentrations were measured by fusion/gas analysis (Inductar). The results are listed in Table 1.These compositions were chosen to obtain near-α alloys. Tungsten, tantalum and hafnium were added in small quantities in order to avoid a too-high increase in alloy density. Aluminium was chosen due to its presence in almost all Ti-based alloys. Experiments were also performed on commercially pure titanium (Ti-50) and forged reference materials (Ti6242S and Ti64). The amount of native oxygen and nitrogen in these alloys was measured by instrumental gas analysis (IGA) at Eurofins EAG Laboratories (Tournefeuille, France), the amount of major elements was measured by energy dispersive X-ray spectroscopy (EDX), and the results are included in Table 1.

Table 1: Composition of studied alloys and oxygen and nitrogen composition of reference materials (at. %).

at. %	Ti	Al	Other elements	N	O
Ti-0.5Ta	Bal.	-	Ta: 0.5	0.01	0.31
Ti-2Ta	Bal.	-	Ta: 2.0	0.02	0.36
Ti-0.5W	Bal.	-	W: 0.5	0.01	0.34
Ti-2W	Bal.	-	W: 2.0	0.01	0.38
Ti-10Al	Bal.	9.9	-	0.01	0.41
Ti-10Al-0.5W	Bal.	10.0	W: 0.5	0.02	0.39
Ti-10Al-2W	Bal.	9.7	W: 2.1	0.01	0.51
Ti-10Al-0.5Ta	Bal.	10.0	Ta: 0.5	0.02	0.44
Ti-10Al-2Ta	Bal.	9.8	Ta: 2.0	0.01	0.45
Ti-10Al-0.5Hf	Bal.	10.2	Hf: 0.5	0.01	0.36
Ti-50 (Grade 2)	Bal.	-	-	0.008	0.269
Ti64	Bal.	10.0	V: 4.1	0.102	0.535
Ti6242S	Bal.	10.5	Zr: 2.1 / Mo: 1.0 Sn: 0.7 / Si: 0.2	0.009	0.228

Samples for oxidation experiments were cut from ingots as thin plates of approximately 13 × 8 × 2 mm^3, and a 2.5 mm diameter hole was drilled to hang each sample in the furnace using an alumina rod. Prior to oxidation, the samples were ground using P600 SiC papers on faces, edges and corners to limit scale spallation. They were finally cleaned in ethanol in an ultrasonic bath and dried in air. The samples were weighed three times using a SARTORIUS LA75 3200D balance with an accuracy of ±20 µg.

Experiments and characterization

Oxidation treatments under laboratory air were performed in a CARBOLITE CWF1300 furnace up to 5000 h at 650 °C with natural convection. Samples were hung in the furnace using an alumina rod. The experiment was interrupted for weighing at intermediate exposure times. Two samples of each alloy were included: one was taken out after 500 h and the other after 5000 h. Oxidation treatments in 80%Ar-20%O_2 were performed in an oxidation bench developed in the laboratory, with a gas flux of 51 mL.min^{-1} corresponding to a gas velocity of 1.2×10^{-4} m.s^{-1} at room temperature, for durations up to 500 h. Samples were hung in the furnace using a preoxidized FeCrAl wire.

The samples were analyzed by grazing-angle XRD at room temperature before the experiments and after some of the interruptions. The measurements were performed using a Bruker RX D8 GIXRD, with a Cu-Kα source. The XRD patterns were acquired in the 2θ range comprised between 10° to 120°, with a step size of 0.02°, a scan step time of 1 s and a low and fixed incident angle of 5°.

After oxidation, copper was electrodeposited on the samples in order to protect the oxide layer. Cross-sections were then cut, mounted, ground with P600 and P1200 SiC paper and then automatically polished using STRUERS DiaPro 9, 3 and 1 µm diamond solutions. They were rinsed with water between each diamond solution, cleaned into ethanol under ultrasounds and dried in air.

All the observations were realized using a FEI Quanta 450 SEM. For the microstructural observations of the raw materials, a further polishing step (using OPS + H_2O_2) was added after the procedure indicated above. From the cross-section SEM images, the average oxide scale thicknesses were calculated by measuring the oxide surface area divided by the length of the oxide scale. The total length of the oxide scale used to determine its thickness on several images is about 300 µm.

Electron-probe microanalysis (EPMA) was carried out to measure composition profiles from the oxide scale to the bulk material. This was done at the R. Castaing Microanalysis Centre (Toulouse, France) with a CAMECA SX Five FE operating at 15 kV and 20 nA. The samples were metallized with C prior to the analysis. The time interval between polishing and C metallization was less than 1 h. Nevertheless, the analysis needs to be corrected by removing the signal due to the native oxide layer and the possible interference of Ti Lβ and O Kα. To do so, the oxygen concentration was measured 5 times in the bulk and set to be equal to 0. This procedure has been described in the work of Casadebaigt [24], and an evaluation of the error made by fixing the native O concentration to 0 was realized. The same correction was applied to all points of the profile; three profiles were measured in each sample.

Oxygen diffusivities given in the following are the average values obtained by fitting these three profiles with an error function (Equation 3). Uncertainty of measurements are taking into account the error realized by fitting profiles and the spread of these 3 results.

Results

Microstructures

Figure 1 shows the microstructures of the model and reference alloys. It should be noticed that the model alloys studied were not heat-treated after the fabrication process. This choice was motivated by the study of Vande Put et al. on Ti6242S who showed that the oxidation kinetics and hardness profiles of Ti-based alloys with similar α-phase fractions are not affected by the morphology of the microstructure [25]. No effect of α-phase laths thickness was also found by Casadebaigt et al. on Ti64 [6]. The model alloys mostly consist of lamellar α/α' phase with very small β phase fraction. The martensite α' is thought to disappear, as shown for Ti64 [6], in the first moments of oxidation at high temperature. The β phase fraction of Ti64 was evaluated to be 10%, and of Ti6242S to be about 16% [26]. For model alloys, the β phase fraction is small and difficult to evaluate. Thermodynamic calculations using ThermoCalc software with TcTi3 database [27] estimated β phase fractions at 650 °C not higher than 2% for Ti-2W alloy.

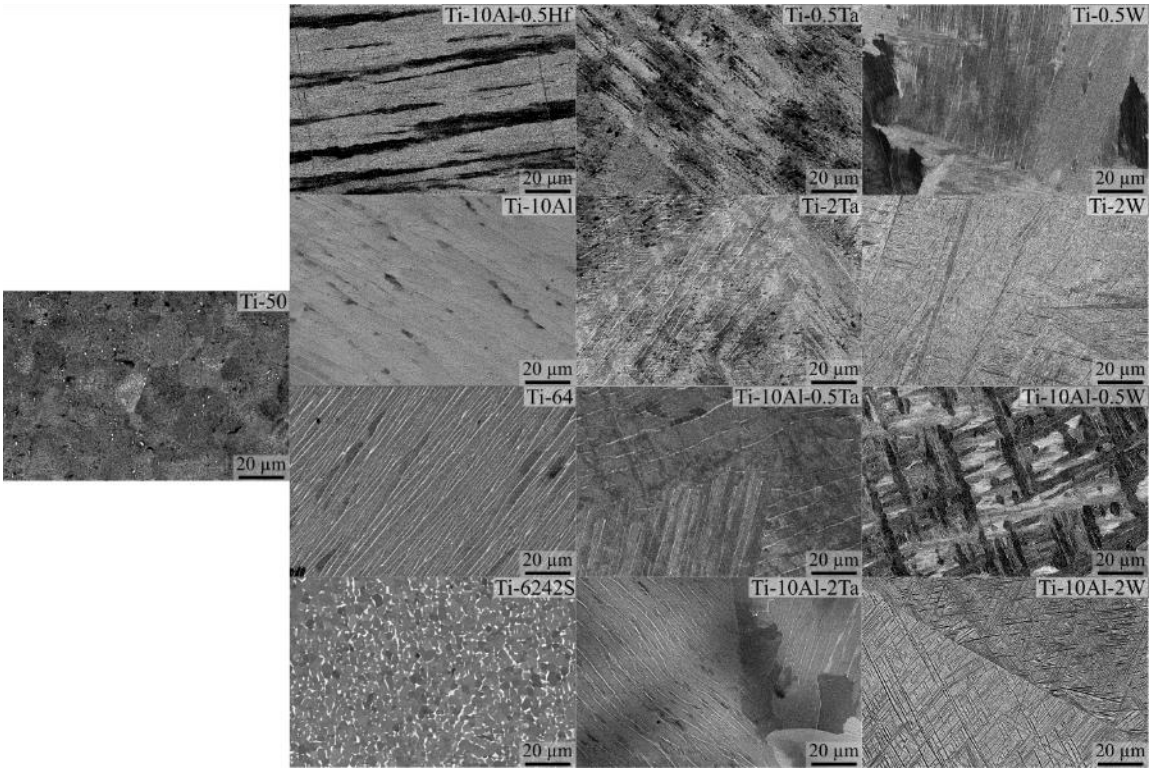

Figure 1: SEM observations of the alloy microstructures (BSE mode).

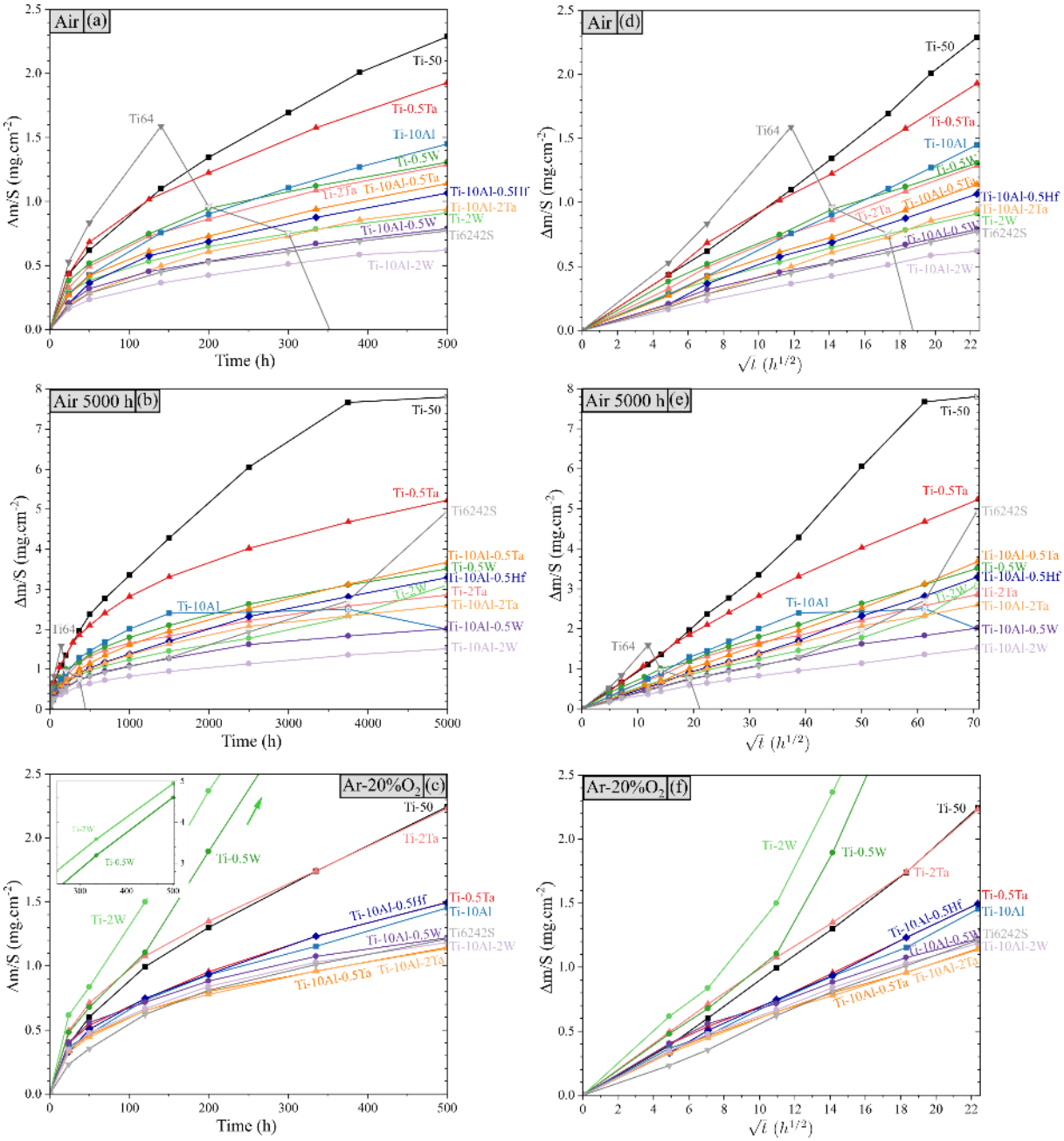

Figure 2: Sample mass change versus time (a-c) or versus square root of time (d-f) for reference and model alloys oxidized at 650 °C for 500 h in air (a, d), for 5000 h in air (b, d) and in Ar-20%O_2 for 500 h (c, f). The insert (c) highlights the total mass gain for Ti-W alloys.

Oxidation kinetics

The mass changes obtained by discontinuous weighing at 650 °C in air and in Ar-20%O_2 are presented in Figure 2. It should be noticed that for oxidation in air up to 500 h, mass gains were obtained with two different samples. The largest difference of mass gains between the two samples oxidized in air for 500 h is 0.08 $mg.cm^{-2}$ for Ti-50, which is less than 5 % of the total mass gain. This proves the repeatability of the experiment. It can be seen that the Ti64 alloy loses mass after 200 h in air: this is due to oxide spalling, which was observed during cooling, before weighing. The alloying elements greatly affect the mass change in both oxidation environments.

In air, Ti-50 has the highest oxidation rate, if Ti64 is excluded. The addition of alloying elements (Al, Ta, W or Hf) always decreases the oxidation rate. The decrease of the oxidation rate is positively correlated to the increase of the element concentration, at least for the small composition range studied here.

Most oxidation kinetics are parabolic, i.e. the mass gains evolve linearly on Figure 2d-f. Nevertheless, some slight decreases of slopes can be observed after about 200 h for the most oxidation-resistant alloys. Also, for the alloys with the highest mass gains, the oxidation kinetics become linear (Figure 2a-c). This change of oxidation behaviour is well known for pure Ti at around 650 °C [8]. The change from parabolic to linear kinetics is observed here for Ti64 and Ti-50 for oxidation in air (Figure 2a-b) and for Ti-W binary alloys in Ar-20%O_2 (Figure 2c). For these alloys, spallation was eventually observed.

Parabolic weight gain kinetics were analysed using the complete parabolic law [28]:

$$t = A + B\left(\frac{\Delta m}{S}\right) + \frac{1}{k_p}\left(\frac{\Delta m}{S}\right)^2 \quad (1)$$

where A and B are coefficients which depend on the transient oxidation regime before the pure parabolic regime. This law was used because of the changes of slopes identified in Figure 2d-f. Indeed, Equation 1 allows to determine k_p in any given range of time [28].

Table 2 gives the parabolic constant k_p for air oxidation, obtained by fitting Equation 1 to the experimental data in time ranges where oxidation kinetics are parabolic. The k_p of the Ti-10Al-2W alloy is ten times lower than that of pure Ti for a short oxidation exposure (< 200 h); the difference is even greater after longer exposure times.

Closer examination of the mass gain curves and of Table 2 shows that W is the most effective element among those tested with regard to decreasing the oxidation rate in terms of mass gain. Tantalum and hafnium have a lesser effect, with Ti-2Ta and Ti-0.5W alloys exhibiting very similar oxidation kinetics in air. In ternary alloys, there is always a positive correlation between Al and the refractory element in decreasing the oxidation rate. It is important to underline that one model alloy, Ti-10Al-2W, has a lower oxidation rate than Ti6242S, which is one of the most oxidation-resistant Ti-based alloys.

In Ar-20%O_2, all tested alloys follow a parabolic oxidation law except the Ti-W binary alloys that follow a linear oxidation law. For these, a breakaway of oxidation kinetics occurs at an early stage of oxidation (for Ti-2W, Ti-0.5W, Ti-2Ta and Ti-50 after 50 h, 100 h, 200 h and 200 h respectively), without visible oxide spallation. In the literature, this oxidation behaviour is related to a very thick multi-layered TiO_2 oxide scale [29]. This is

confirmed by cross-section observations presented in the next section. For all the other alloys, the k_p constants related to the oxidation in Ar-20%O_2 are also given in Table 2. The differences among the k_p constants determined for the different alloys in Ar-20%O_2 are less important than those observed in air.

The ratio of k_p values between Ar-20%O_2 and air up to 500 h shows that the oxidation rates are always greater in Ar-20%O_2 than in air, except for Ti-0.5Ta, without any explanation yet for this particular alloy. For Ti-50, there is no significant change in oxidation kinetics between the two atmospheres, which is unexpected, since previous studies reported higher oxidation rates in Ar-20%O_2 than in air [30].

Except for Ti-50, the k_p values measured here are in good agreement with previous studies for Ti6242S and model alloys.

Table 2: Parabolic constants k_p of model and reference alloys oxidized at 650 °C in air up to 5000 h and in Ar-20%O_2 up to 500 hours, and k_p values from litterature for comparison. Durations in parentheses indicate the range where k_p values are calculated.

Alloys	Air k_p (10^{-7} mg².cm^{-4}.s^{-1})		Ar-20%O_2 [0 – 500 h] k_p (10^{-7} mg².cm^{-4}.s^{-1})	$\frac{k_p(Ar-20\%O_2)}{k_p(Air)}$ [0 - 500 h]
Ti-50	38 [0 – 690 h]	63 [690 – 3750 h]	25	1.5
Ti-10Al	9.6 [0 - 1500 h]		12	1.3
Ti-10Al-0.5Ta	7.9 [0 - 5000 h]		8.2	1.0
Ti-10Al-2Ta	4.5 [0 - 1500 h]	1.2 [1500 – 5000 h]	6.8	1.5
Ti-10Al-0.5W	3.9 [0 - 370 h]	1.1 [370 – 5000 h]	9.9	2.5
Ti-10Al-2W	2.1 [0 - 200 h]	0.8 [200 – 5000 h]	8.9	4.2
Ti-10Al-0.5Hf	6.4 [0 - 5000 h]		12	1.9
Ti-0.5Ta	24 [0 - 500 h]	8.3 [500 - 5000 h]	12	0.5
Ti-2Ta	9.4 [0 - 500 h]	2.9 [500 - 5000 h]	27	2.9
Ti-0.5W	12 [0 - 200 h]	5.0 [200 – 5000 h]	N/A	N/A
Ti-2W	5.6 [0 - 200 h]	2.1 [200 – 2500 h]	N/A	N/A
Ti6242S	2.5 [0 – 1500 h]		8.4	3.4
Ti64	45 [0 – 150 h]	-	-	-
Ti-50 [30, 31]	18 | 47.2 [0 – 1000 h]		51 [100 – 300 h]	-
Ti64 [5, 32]	38 | 43 [0 – 300 h]		-	-
Ti6242S [31, 33]	1.9 [0 – 100 h] | 3.2 [0 – 1000 h]		10 [0 – 100 h]	-
Ti-8.5at.%Al [8]	15 [0 – 800 h]		-	-
Ti-0.8at.%W [23]	14.6 [0 – 300 h]		-	-

For some alloys, there is a change in k_p values during the exposure, which suggests the succession of two parabolic laws, as shown in Figure 2d and e and listed in Table 2. The k_p values for pure titanium strongly increase at longer durations. These alloys exhibit a breakaway of the mass uptake, and oxide spallation is visible for Ti-10Al, pure titanium and Ti6242S at the very end. Berthaud studied the oxidation of Ti6242S at 560 °C up to 19 kh and showed a sharp increase of the mass gain between 10 and 19 kh [34]. This breakaway is similar to those observed in this study.

The comparison between the oxidation rates in air and in Ar-20%O_2 reveals an important role of the alloying elements on the overall mass gain. It is therefore important to perform finer analyses on the oxide scale and on the O diffusion zone, to better understand the effects of the alloying elements.

Analysis of the oxide scale

Figure 3a shows the X-rays diffraction patterns of the alloys oxidized in air at 650 °C, for 500 hours. For all alloys, the only oxide detected is TiO_2 rutile (space group: N° 136). No Al_2O_3 alumina peaks are detectable for Ti-10Al and ternary alloys, even though a thin Al-rich layer was observed on top of the TiO_2 scale on EDS maps (not shown here). The hexagonal α phase from the matrix is also detected by XRD, with an increase in lattice parameters after oxidation. This is due to the large O dissolution in the alloy just below the oxide scale [35]. For some alloys, the β phase can be identified from weak peaks. Only for model alloys containing W, another phase is observed. This has been identified as a Ti_2N nitride with anti-rutile structure (space group: N° 136, ICDD 01-076-0198). Diffraction patterns measured after 50 h of exposure in air also reveal the presence of titanium nitride in alloys containing 2 at. % W, as shown in Figure 3b. A last low-intensity XRD peak located at 2θ =42.6-42.7° remains unidentified for some alloys. It could be attributed to TiN, TiO or TiO_xN_y fcc-structure without certainty (such as TiN_{1-x} ICDD 01-087-0631, TiO_{1-x} ICDD 00-008-0117 or $TiO_{1-x}N_x$ ICDD 01-084-4872 with lattice parameters refinements).

Cross-sectional SEM images (Figure 4) were used to measure oxide scale thicknesses, given in Table 3. In air, the oxide scale thickness decreases by adding alloying elements. The oxide scales grown on Ti-W alloys are twice as thin as those grown on Ti-Ta alloys. The oxide scales are also a little bit thinner in Ti-Al-W alloys compared to

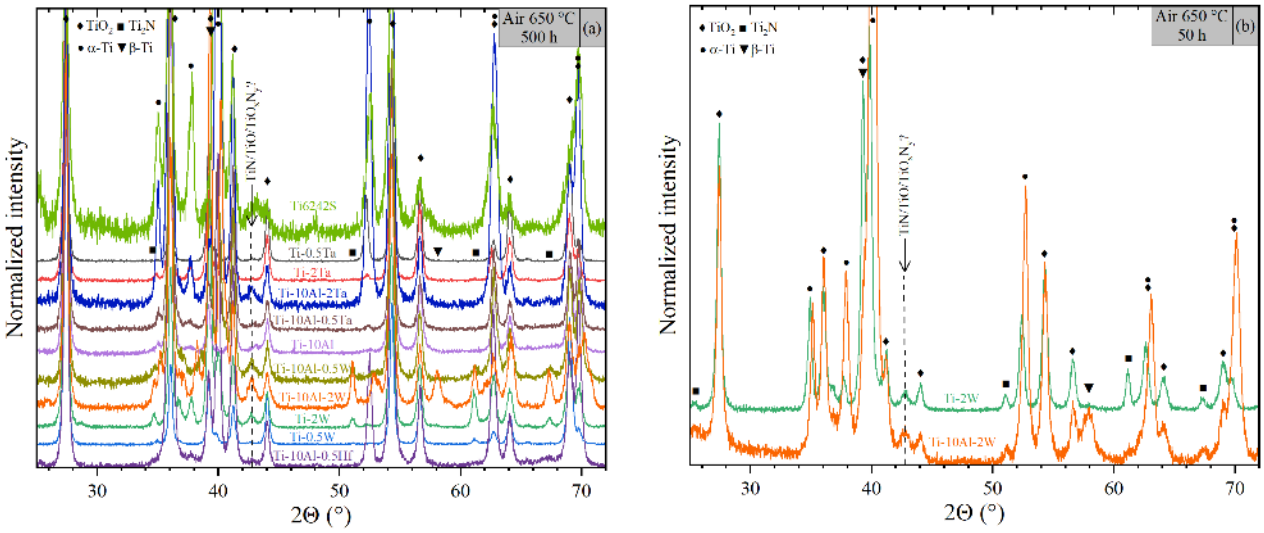

Figure 3: XRD analyses with a low incidence angle of 5° for a): model alloys and Ti6242S oxidized 500 h at 650 °C in air and for b): Ti-2W and Ti-10Al-2W alloys oxidized 50 h at 650 °C in air, indicating Ti_2N peaks at the early stage of oxidation. All XRD spectra are normalized to the same (110) TiO_2 peak intensity at 2θ=27.4°.

Ti-Al-Ta or Ti-Al-Hf alloys. After 5000 h of oxidation in air for some alloys, not shown here, the oxide scale is porous and layered, which can lead to oxide scale spallation. For Ti-10Al, two distinct thicknesses were observed at different locations on the same sample, due to oxide spallation.

Table 3: Comparison of oxide scale thicknesses with oxide mass gain $(\Delta m/S)_{ox}$ for the alloys oxidized at 650 °C for 500 h in air and in Ar-20%O_2. †: For these alloys, the oxide thickness considers voids between thin layers. This void proportion was estimated to be about 15% for Ti-W alloys by image analysis and was taken into account to calculate $(\Delta m/S)_{ox}$.

Alloys	Air			Ar-20%O_2		
	Oxide thickness (µm)	$(\Delta m/S)_{ox}$ (mg.cm^{-2})	$(\Delta m/S)_{ox}/(\Delta m/S)_{tot}$ (%)	Oxide thickness (µm)	$(\Delta m/S)_{ox}$ (mg.cm^{-2})	$(\Delta m/S)_{ox}/(\Delta m/S)_{tot}$ (%)
Ti-50	7.6 ± 0.7	1.29 ± 0.12	56 ± 5	16.1 ± 0.8	2.73 ± 0.15	121 ± 7
Ti-10Al	4.7 ± 0.4	0.80 ± 0.07	55 ± 5	4.0 ± 0.4	0.68 ± 0.07	47 ± 5
Ti-10Al-0.5Ta	2.6 ± 0.1	0.44 ± 0.02	39 ± 2	3.4 ± 0.3	0.58 ± 0.04	51 ± 4
Ti-10Al-2Ta	1.7 ± 0.2	0.29 ± 0.03	31 ± 4	2.4 ± 0.3	0.41 ± 0.05	36 ± 4
Ti-10Al-0.5W	2.0 ± 0.3	0.34 ± 0.05	43 ± 6	3.3 ± 0.2	0.56 ± 0.03	46 ± 3
Ti-10Al-2W	1.4 ± 0.1	0.24 ± 0.02	39 ± 3	3.6 ± 0.2	0.60 ± 0.03	51 ± 3
Ti-10Al-0.5Hf	3.1 ± 0.1	0.53 ± 0.02	49 ± 2	4.3 ± 0.3	0.73 ± 0.05	49 ± 3
Ti-0.5Ta	6.1 ± 0.3	1.03 ± 0.05	54 ± 3	4.5 ± 0.4	0.75 ± 0.07	50 ± 5
Ti-2Ta	3.7 ± 0.2	0.63 ± 0.03	49 ± 3	8.7 ± 0.5	1.47 ± 0.08	66 ± 4
Ti-0.5W	3.2 ± 0.5	0.54 ± 0.06	42 ± 5	37.7 ± 1.0†	5.42 ± 0.31	118 ± 7
Ti-2W	2.0 ± 0.2	0.34 ± 0.03	37 ± 4	40.3 ± 1.1†	5.81 ± 0.33	118 ± 7
Ti6242S	1.1 ± 0.1	0.18 ± 0.02	23 ± 2	3.4 ± 0.5	0.57 ± 0.08	47 ± 7

Following the same approach as Vaché et al. [5], the overall mass gain was broken down into several contributions. As shown before, the mass of O dissolved in the metal $\left(\frac{\Delta m}{S}\right)_{O\ in\ Ti}$ cannot be neglected in front of the mass of oxygen in the external oxide scale $\left(\frac{\Delta m}{S}\right)_{O\ in\ TiO_2}$. In the present study, we added the nitrogen contribution, because nitrides were sometimes identified by XRD. Nitrogen is present in the nitrides $\left(\left(\frac{\Delta m}{S}\right)_{N\ in\ Ti_2N}\right)$, but it can also be dissolved in quite large quantities in the metal $\left(\left(\frac{\Delta m}{S}\right)_{N\ in\ Ti}\right)$ [36]. Therefore, the complete mass gain of the samples can be written as follows:

$$\left(\frac{\Delta m}{S}\right)_{tot} = \left(\frac{\Delta m}{S}\right)_{O\ in\ TiO_2} + \left(\frac{\Delta m}{S}\right)_{O\ in\ Ti} + \left(\frac{\Delta m}{S}\right)_{N\ in\ Ti_2N} + \left(\frac{\Delta m}{S}\right)_{N\ in\ Ti} \quad (2)$$

It should be noticed that Equation 2 does not take into account the mass gain of N in the oxide scale and of O in the nitride scale. This is supported by previous studies that measured very low concentration of N in TiO_2 and O in titanium nitrides [36, 37]. The oxygen intake in the oxide scale can be computed from the oxide thickness, assuming a continuous, homogeneous, fully compact and adherent oxide scale TiO_2, using the Equation 2:

$$\left(\frac{\Delta m}{S}\right)_{O\ in\ TiO_2} = \frac{t_{ox} * \rho_{TiO_2} * 2 * M_O}{M_{TiO_2}} \quad (3)$$

with t_{ox} the oxide scale thickness, ρ_{TiO_2} the oxide density, M_O and M_{TiO_2} the molar weight of oxygen and TiO_2.

The mass gain due to the oxide growth is also reported in Table 3 for 500 h of oxidation, and in Table 4 for 5000 h of oxidation in air. The part of the oxygen mass gain due to the oxide scale over the total mass gain remains constant between 500 and 5000 h for Ti6242S, Ti-0.5Ta, Ti-10Al-W and Ti-10Al-2Ta, while it increases with time for pure titanium. This is due to linear kinetics of oxide scale growth rate for Ti-50, whereas the kinetics of oxygen dissolution in the metal remains parabolic.

Table 4: Oxide scale thicknesses with oxide mass gain $(\Delta m/S)_{ox}$ for the alloys oxidized at 650 °C for 5000 h in air. †: For these alloys, the oxide thickness considers voids between thin layers. This void proportion was estimated by image analysis to calculate $(\Delta m/S)_{ox}$.

Alloys	Air 5000 h		
	Oxide thickness (µm)	$(\Delta m/S)_{ox}$ (mg.cm^{-2})	$(\Delta m/S)_{ox}/(\Delta m/S)_{tot}$ (%)
Ti-50	45.1 ± 1.5†	6.11 ± 0.25	78 ± 3
Ti-10Al	-	-	-
Ti-10Al-0.5Ta	10.6 ± 0.2	1.79 ± 0.03	49 ± 1
Ti-10Al-2Ta	5.6 ± 0.5	0.96 ± 0.08	37 ± 3
Ti-10Al-0.5W	5.5 ± 0.2	0.92 ± 0.03	46 ± 2
Ti-10Al-2W	3.5 ± 0.3	0.59 ± 0.05	39 ± 3
Ti-10Al-0.5Hf	12.7 ± 0.5	2.16 ± 0.08	66 ± 3
Ti-0.5Ta	19.5 ± 0.5†	3.04 ± 0.10	58 ± 2
Ti-2Ta	6.8 ± 0.3	1.14 ± 0.05	40 ± 2
Ti-0.5W	10.7 ± 0.3	1.81 ± 0.03	51 ± 2
Ti-2W	10.3 ± 0.2	1.75 ± 0.03	56 ± 1
Ti6242S	6.5 ± 0.4	1.11 ± 0.07	22 ± 2

Oxide scales grown on Ti-W alloys in Ar-20%O_2 consist of many thin layers of about 1 µm, forming a final oxide scale of 30 to 40 µm. This observation is expected, given the linear kinetics observed in Figure 2b. Micrographs of Ti-2W showing the comparison between air and Ar-20%O_2 are presented in Figure 5. Stringer observed the layering of oxide scales on pure titanium and explained it with stress accumulation [38]. In our work, multi-layered oxide formation is observed on binary Ti-W alloys under oxygen but not under air. This difference of oxide morphology associated with the reaction gas has also been reported by Dupressoire et al. on Ti6242S [33]. These authors attributed the delamination under oxygen to the larger oxidation rate in this gas, which favored the earlier attainment of the critical thickness that causes the oxide layer to detach. In Ar-20%O_2, oxide thicknesses increase for all alloys by comparison to air oxidation treatment, except for Ti-0.5Ta alloy, where the oxide scale is thinner in Ar-20%O_2 than in air oxidation (4.5 µm vs. 6.1 µm respectively).

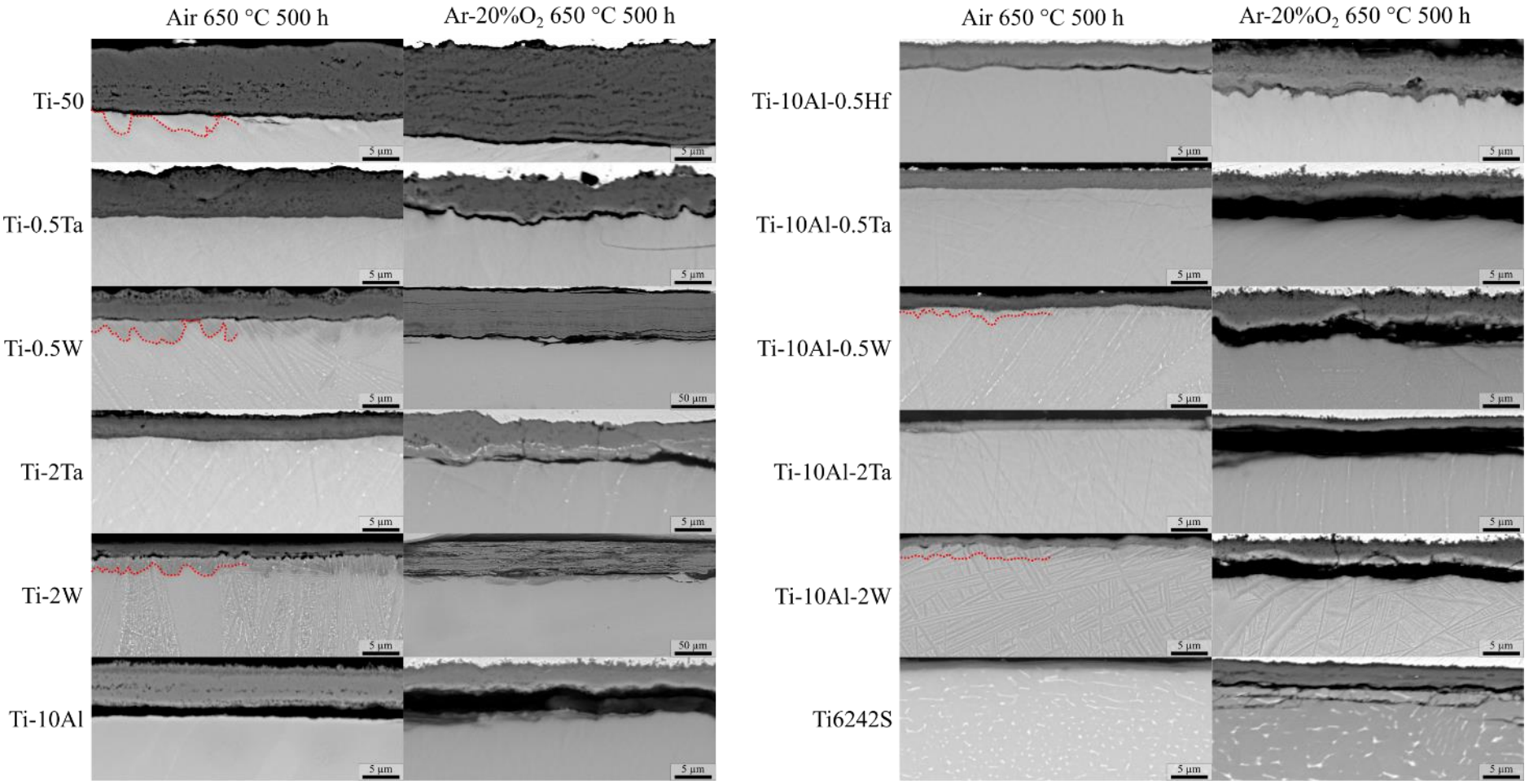

Figure 4: SEM images (BSE mode) of oxide scales for alloys oxidized in air or Ar-20%O_2 at 650 °C for 500 h. Scale bars correspond to 5 µm, except Ti-W binary alloys oxidized in Ar-20%O_2 which correspond to 50 µm. Red dotted lines indicate the nitride/metal interface.

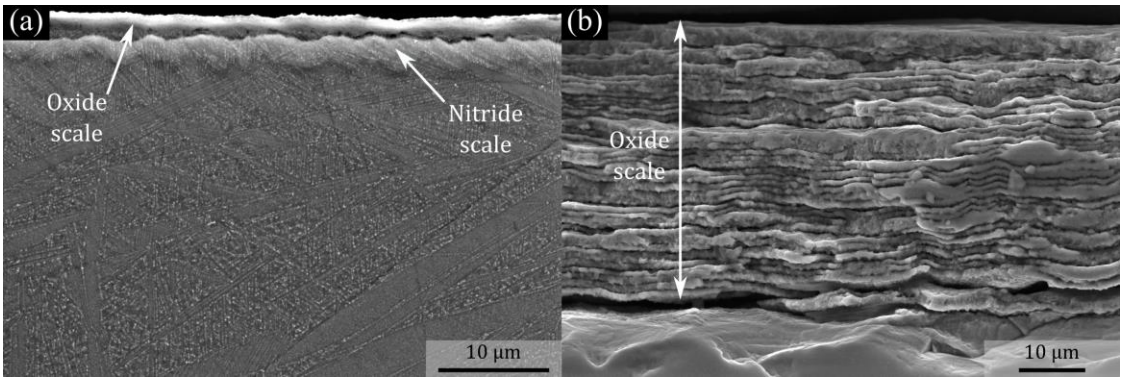

*Figure 5: SEM image (SE mode) of the cross-section of the oxide scale formed on the Ti-2W alloy after 500 h at 650 °C **(a)** in laboratory air and **(b)** in Ar-20%O_2.*

Oxygen diffusivity

Oxygen profiles obtained using EPMA on alloys oxidized for 500 h and 5000 h at 650 °C in air and for 500 h in Ar-20%O_2 are shown on Figure 6. On initial observation, one can remark that the oxygen penetration lengths are similar for all the alloys. Assuming that the alloy is a semi-infinite, pseudo-binary metal-oxygen system, with a constant concentration at its surface, and using Fick's law with a constant interdiffusion coefficient, the solution of the diffusion problem is [39]:

$$C(x) = C_0 + (C_s - C_0) * \left(1 - \mathrm{erf}\left(\frac{x}{2\sqrt{Dt}}\right)\right) \quad (4)$$

where C_0 and C_s are oxygen concentration in the bulk and at the oxide/alloy interface respectively, D the interdiffusion coefficient, t the oxidation time and x the depth from the metal surface. Inasmuch as the oxygen diffusivity is four decades larger than that of Ti and of the alloying elements at 650 °C (calculated using Thermo-Calc [27] and the MOBTI3 database [40]), the inter-diffusion coefficient is approximately equal to the intrinsic diffusion coefficient of oxygen.

Oxygen diffusivities and concentrations at the metal surface obtained by fitting Equation 4 to the experimental profiles are given in Table 5.

Oxygen diffusivity values are close to those obtained in previous studies. Indeed, Shenoy et al. measured, by microhardness profiles, the O diffusivity which is equal to 1.74×10^{-16} m².s^{-1} in Ti6242S oxidized at 649 °C [7]. David et al. measured the O diffusivity by nuclear resonance analysis and obtained a value of 4.2×10^{-17} m².s^{-1} in pure Ti heat treated at 648 °C [41], which is a little bit lower than our value.

Table 5: Oxygen diffusivity D and oxygen concentration in the metal at the oxide/alloy interface C_s of model and reference alloys oxidized in air for 500 and 5000 h, and in Ar-20%O_2 at 650 °C up to 500 hours.

Alloys	Air 500 h D (10^{-17} $m^2.s^{-1}$)	Air 500 h C_s (at. % O)	Air 5000 h D (10^{-17} $m^2.s^{-1}$)	Air 5000 h C_s (at. % O)	Ar-20%O_2 D (10^{-17} $m.s^{-1}$)	Ar-20%O_2 C_s (at. % O)
Ti-50	18 ± 2	25 ± 1	12 ± 1	26 ± 1	13 ± 2	26 ± 1
Ti-10Al	6.0 ± 0.6	25 ± 2	5.9 ± 0.5	25 ± 1	8.1 ± 0.8	26 ± 1
Ti-10Al-0.5Ta	8.5 ± 0.7	27 ± 1	8.3 ± 0.7	25 ± 1	6.8 ± 0.8	27 ± 2
Ti-10Al-2Ta	13 ± 3	22 ± 2	14 ± 1	16 ± 1	6.8 ± 0.6	27 ± 2
Ti-10Al-0.5W	12 ± 3	15 ± 1	18 ± 3	6.1 ± 1.8	7.9 ± 1.3	27 ± 1
Ti-10Al-2W	13 ± 4	8.8 ± 1.0	17 ± 3	7.0 ± 1.2	7.3 ± 1.6	25 ± 1
Ti-10Al-0.5Hf	11 ± 2	22 ± 2	13 ± 1	14 ± 1	9.0 ± 1.9	26 ± 2
Ti-0.5Ta	21 ± 2	29 ± 1	23 ± 3	23 ± 1	23 ± 1	19 ± 2
Ti-2Ta	20 ± 3	20 ± 1	17 ± 4	11 ± 3	12 ± 2	25 ± 2
Ti-0.5W	21 ± 3	16 ± 1	20 ± 2	11 ± 2	8.6 ± 1.9	26 ± 2
Ti-2W	21 ± 3	8.7 ± 1.2	14 ± 3	13 ± 3	7.8 ± 0.5	28 ± 1
Ti6242S	11 ± 1	23 ± 1	6.4 ± 0.6	25 ± 1	12 ± 2	33 ± 3

Aluminium decreases the O diffusivity in Ti-10Al by a factor of 3 in comparison to pure titanium. Tantalum and tungsten slightly increase the O diffusivity in the α phase. Nevertheless, tungsten decreases the O concentration at the oxide/metal interface for oxidation in air, whereas C_s remains high for other alloying elements in air, and for Ar-20%O_2 oxidation treatment.

In air and in Ar-20%O_2, ternary alloys have lower O diffusivities than pure titanium and binary alloys. This lowering effect is probably due to the Al addition as seen in the Ti-10Al alloy. The slightly higher O diffusivity values observed for the ternaries in comparison to the Ti-10Al binary indicates that the refractory elements slightly increase the O diffusivity. For 5000 h exposition in air, the O diffusivity is almost the same than for 500 h, except for Ti6242S, which is yet to be explained. Nevertheless, the main change between the two durations in air concerns the C_s values, which considerably decrease for Ti-0.5/2Ta, Ti-10Al-2Ta, Ti-10Al-0.5W and Ti-10Al-0.5Hf alloys. For instance, for Ti-10Al-0.5W, C_s decreases from 15 ± 1 at. % at 500 h to 6.1 ± 1.8 at. % at 5000 h. In Ar-20%O_2, the O diffusivity is almost the same for some alloys (Ti-50, Ti-10Al, Ti-0.5Ta, Ti-10Al-0.5Ta/Hf), whereas the value is lower for the other alloys.

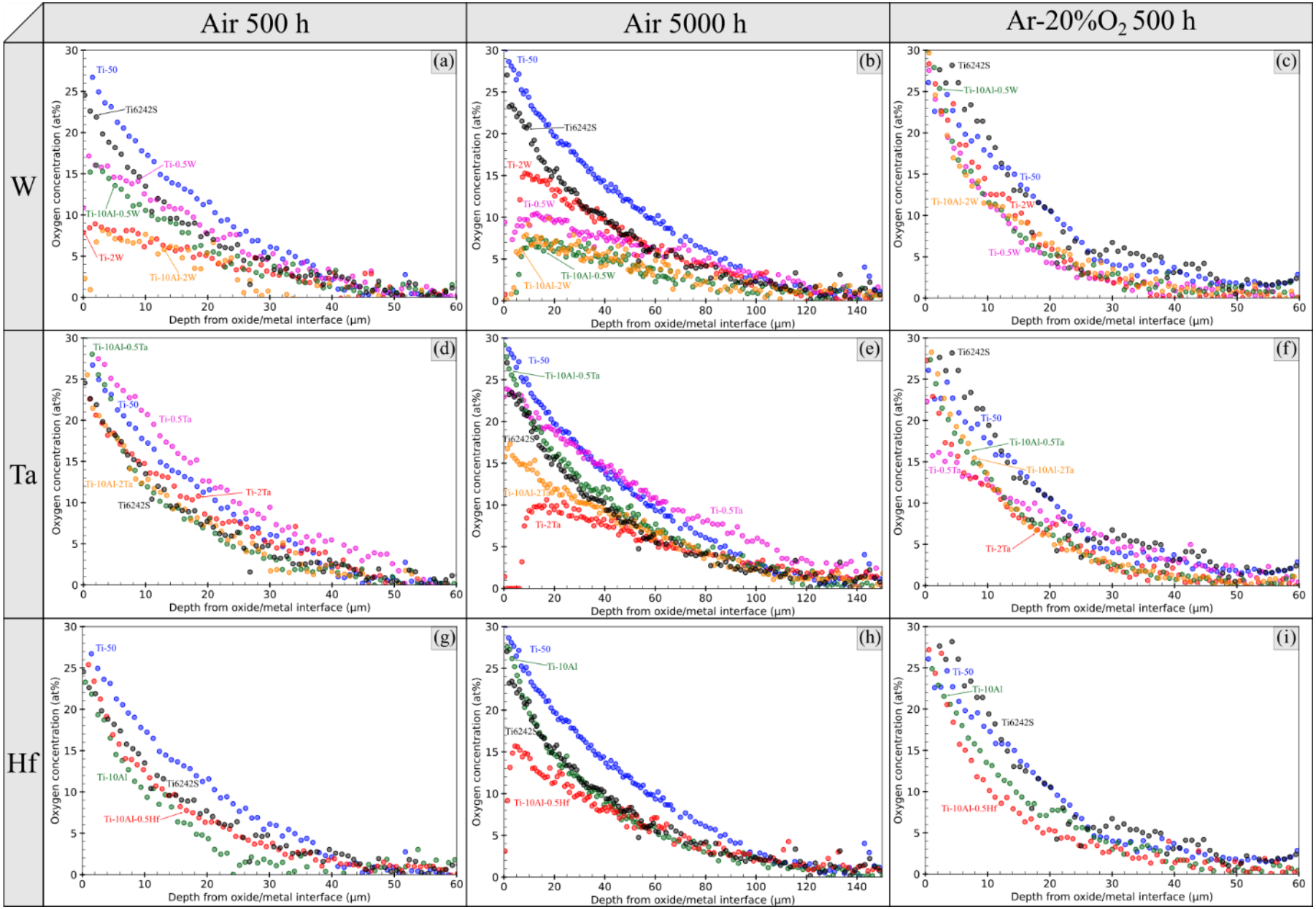

Figure 6: EPMA oxygen penetration profiles for alloys oxidized at 650°C in air for 500 h (a, d and g), for 5000 h (b, e, h) and in Ar-20%O_2 for 500 h (c, f and i).

The oxygen concentration profiles obtained on the Ti-W and Ti-10Al-W alloys oxidized in air (and not in Ar-20%O_2) exhibit a significant change of the oxygen concentration in the alloy just below the oxide scale compared to pure titanium. Indeed, for 500 h of oxidation in air, by increasing the W content in the alloy, C_s decreases from 25 at. % to around 15 at. % and 9 at. % for 0.5W and 2W respectively. The C_s values become equal after 5000 h in air for both ternary Ti-Al-W alloys, i.e. about 8 at. %. This decrease does not occur for the Ar-20%O_2 oxidation treatments. This observation shows that the presence of W alone does not explain the decrease of the O content dissolved in α-Ti: the decrease of C_s is due to the simultaneous presence of W in the alloy and nitrogen in the oxidant gas. For the Ti-2W alloy, we observed an unexpected increase of C_s value from 8 to 13 at. % from 500 h to 5000 h.

It should be noticed that due to the decrease of the oxygen concentration in the alloy just below the oxide scale, the use of the erf function solution (Equation 4) to determine the O diffusivities in Ti-(Al)-W alloys oxidized in air is not strictly correct. Indeed, this solution assumes a constant concentration at the alloy surface, which is not the case for these alloys. For all alloys in this particular case, Equation 4 was fitted from the maximum O concentration of each profile, and the position $x = 0$ of these profiles was fixed at the maximum of the O concentration peak.

Nitride formation

On the cross-sections of some alloys, titanium nitride Ti_2N can be identified just below the oxide scale by EBSD, SAED and EDS-TEM (not shown here). The presence of titanium nitrides was already observed in previous studies [30, 36, 42, 43]. Chaze and Coddet proposed an explanation on the location of the nitride below the oxide scale based on differences in O and N diffusivities in the oxide and in the metal. They assumed that the diffusion of nitrogen in rutile TiO_2 was faster than that for oxygen as proposed in [43, 44], and they recognized that oxygen diffuses more than ten times faster than nitrogen in the metal [45, 46]. This should leads to an accumulation of nitrogen in the metal, just below the oxide scale, which can lead to nitride precipitation as observed. Depending on the alloy, the nitride forms a continuous layer, as shown in Figure 5a, or a discontinuous one, as visible on the micrographs of Ti-50 and Ti-0.5W oxidized in air for 500 h (Figure 4). The thickness of the nitride layer is also variable in the various alloys. To find out the contribution of N in Ti_2N to the total mass gain, the surface covered by nitrides was estimated by image analysis from 10 SEM images, in SE mode, for each alloy. Figure 7 shows a box plot representing the Ti_2N thickness distribution for each alloy treated in air, for 500 h at 650 °C. It should be noticed that titanium nitride thicknesses in this study are significantly higher than those observed in previous studies. In the study of Dupressoire et al., the authors evaluated the nitride thickness in a Ti6242S alloy oxidized

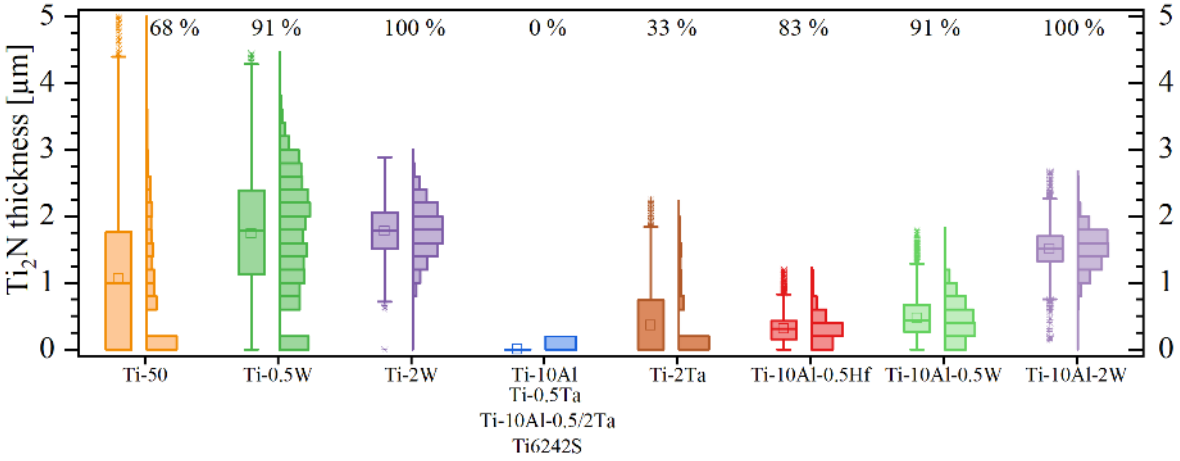

Figure 7: Titanium nitride Ti_2N thickness distribution for each alloy with, at the top of each box, the corresponding surface coverage after 500 h at 650 °C oxidation treatment in air. Square symbols are for the mean value of nitride thickness.

at 650 °C in air, for 1000 hours, to be comprised from dozen to hundreds of nanometers [36]. In pure Ti, Optasanu et al. also showed the presence of a discontinuous nitride layer after 20 h at 700 °C [42].

In the present study, as already mentioned, the nitride layer is not continuous for some of the alloys and it has a "saw-tooth" shape. This particular shape explains the variability of its thickness in e.g. Ti-50 or Ti-2Ta. The reason of this saw-tooth shape, and the overall mechanism of growth of this layer will be discussed in an upcoming paper.

The Ti-10Al alloy does not form any nitride, as also confirmed by EBSD analysis (not shown here). Aluminium visibly has an adverse effect on nitride formation. Indeed, this effect is also visible when comparing binary and ternary alloys containing refractory elements: the mean thickness of the nitride layer is always lower in the ternary alloy- containing Al- than in the corresponding binary alloy (Figure 7). It should be noticed that Al has very low solubility in Ti_2N [47]; Dupressoire et al. measured a dissolved concentration of Al in Ti_2N equal to 1.5 at. % by atomic probe tomography in Ti6242S oxidized in synthetic air for 1000 h at 650 °C [36]. It seems therefore likely that in the Al-containing alloys studied here (10 at. %), nitride growth is slowed down by Al diffusion in the α-phase away from the nitride precipitation front.

Oxygen dissolution in the alloys

The amount of oxygen dissolved in the alloy per unit surface area can be estimated by integrating the oxygen concentration profiles [5]:

$$\left(\frac{\Delta m}{S}\right)_{O-diss} = \int_{x=0}^{+\infty} (C - C_0)dx * \frac{\rho_{Ti-alloy}}{M_{Ti-alloy}} M_O \quad (5)$$

where $\rho_{Ti-alloy}$ is the density of the titanium alloy (in $mg.cm^{-3}$), and $M_{Ti-alloy}$ and M_O are the molar masses of the titanium alloy and oxygen (in $g.mol^{-1}$), respectively. Table 6 gives the mass gains associated with oxygen

dissolution in the metal. In air, after 500 h, the Ti-W binary alloys dissolve less oxygen than pure titanium even though O diffusivities are almost equal (Table 5). This is clearly the result of the decrease in oxygen concentration at the nitride/alloy interface, as shown in Figure 6a. Furthermore, a combined effect of the decrease in O diffusivity due to Al and the decrease in oxygen concentration at the oxide/alloy interface to about 10 at. % O explains the very low amount of O dissolution in Ti-10Al-2W. For very long oxidation treatments in air, W additions are the most efficient to decrease oxygen dissolution. Indeed, Ti-10Al-2W after 5000 h oxidation in air dissolves about the same amount of O than pure titanium in 500 h, or twice less than Ti6242S for the same oxidation duration. These results show clearly the effect of the nitride layer as a diffusion barrier for O. For the Ti-2W alloy, the O concentration at the alloy interface increased from 8 at. % to 13 at. % between 500 and 5000 h. This unexpected result may be attributed to a decrease in the protective properties of the diffusion barrier. The nitride layer undergoes continuous oxidation at the oxide/nitride interface while being formed at the nitride/metal interface. As depicted in Figure 2e, the oxidation rate increases after 3500 h, suggesting that the nitride layer may have oxidized more rapidly thereafter, thereby diminishing the effectiveness of the diffusion barrier.

In Ar-20%O_2, the mass gain due to O dissolution is very close for all model alloys. This further proves that the decrease in the oxygen dissolution in the Ti-10Al-2W alloy is not due to a direct effect of alloying element on O diffusivity nor O solubility. The effect must be related to the formation of nitrides, since this only occurs in air. Indeed, for all the alloys, the presence of nitrogen in the oxidation atmosphere decreases the dissolution of oxygen compared to Ar-20%O_2 atmosphere, with the sole exception of the Ti-0.5Ta alloy, which remains to be explained.

Table 6: Comparison of mass gain associated with the oxygen dissolution measured by integration of EPMA profiles, using Equation 4, between both oxidation treatments (air or Ar-20%O_2).

Alloys	Air 500 h	Air 5000 h	Ar-20%O_2 500 h
	$(\Delta m/S)_{O-diss}$ (mg.cm^{-2})	$(\Delta m/S)_{O-diss}$ (mg.cm^{-2})	$(\Delta m/S)_{O-diss}$ (mg.cm^{-2})
Ti-50	0.77 ± 0.02	2.01 ± 0.05	0.67 ± 0.05
Ti-10Al	0.45 ± 0.05	1.42 ± 0.09	0.54 ± 0.06
Ti-10Al-0.5Ta	0.57 ± 0.03	1.64 ± 0.04	0.51 ± 0.05
Ti-10Al-2Ta	0.56 ± 0.04	1.38 ± 0.11	0.49 ± 0.01
Ti-10Al-0.5W	0.43 ± 0.03	0.73 ± 0.08	0.55 ± 0.06
Ti-10Al-2W	0.28 ± 0.04	0.81 ± 0.01	0.47 ± 0.04
Ti-10Al-0.5Hf	0.53 ± 0.02	1.28 ± 0.04	0.56 ± 0.08
Ti-0.5Ta	0.93 ± 0.01	2.41 ± 0.12	0.65 ± 0.07
Ti-2Ta	0.60 ± 0.02	1.26 ± 0.04	0.57 ± 0.08
Ti-0.5W	0.57 ± 0.03	1.23 ± 0.03	0.53 ± 0.08
Ti-2W	0.33 ± 0.05	1.21 ± 0.16	0.53 ± 0.03
Ti6242S	0.54 ± 0.03	1.39 ± 0.05	0.82 ± 0.05

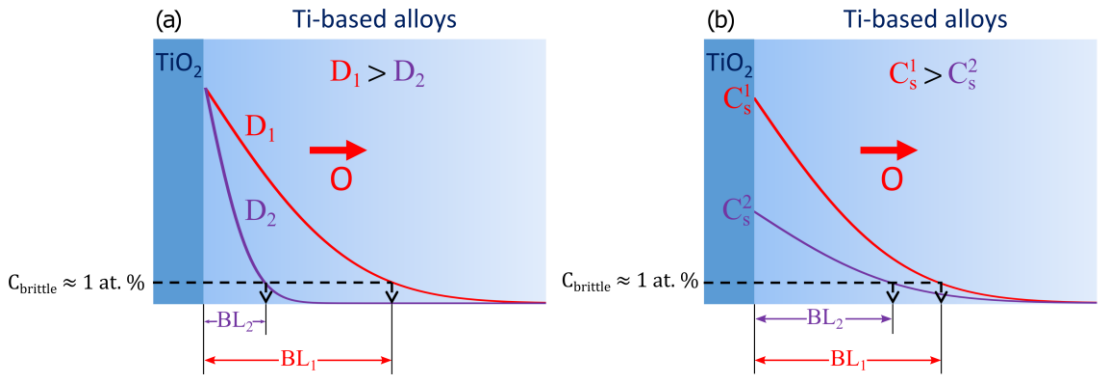

Figure 8: Schematic representation of the effect of (a) oxygen diffusivity decrease, and (b) oxygen solubility decrease on brittle layer (BL) thickness.

Discussion

The objective of studying the effect of alloying elements on oxygen diffusivity and solubility is to reduce the brittle layer thickness due to oxygen ingress. Figure 8 illustrates how the brittle layer thickness is affected by a decrease in oxygen diffusivity (Figure 8a) or in oxygen solubility at the oxide/metal interface (Figure 8b). The oxygen concentration corresponding to the ductile to brittle transition at room temperature, is fixed at about 1 at. % on schematics in Figure 8, but it may vary depending on the alloys and thus should be determined in all new designed alloys.

Distinguishing the oxygen uptake due to scale growth and to diffusion in the alloy, and comparing the results obtained after exposure to air and to Ar-20%O_2, provides a better understanding of the way in which alloying elements affect the oxidation resistance of titanium. A key result of the present work is that none of the refractory alloying elements studied here (tungsten, tantalum, hafnium) markedly affects the diffusivity of oxygen in α-Ti. However, these elements do impact the penetration depth of oxygen in the alloy, due to their effect on the oxygen concentration at the oxide/alloy interface; which in turn is related to nitride precipitation. On the contrary, the addition of aluminium reduces the oxygen diffusivity, without affecting its solubility in α-Ti. The oxide scale thicknesses were also found to be affected by the alloy composition. The importance of these processes in the oxidation resistance is now illustrated by decomposing the total mass gain into individual contributions.

Decomposition of the total mass gain

Figure 9 shows the decomposition of the total mass gain into O and N contributions in the external oxide/nitride scale and in the metal. It was not possible to quantify nitrogen dissolved in the metal by EPMA due to overlapping between N-Kα and Ti-Lα peaks and perhaps also due to the insufficient spatial resolution of EPMA compared to the depth of the N diffusion profile. We therefore estimated the amount of nitrogen dissolved in the metal based on nitrogen diffusivity data in α-Ti from the literature [45, 48, 49], and assuming a N concentration at the nitride/metal interface equal to 20 at. %, as measured by TEM-EDX and APT in Ti6242S alloy [36]. In the absence of composition-dependant diffusivity data, the same estimated value was applied to all alloys.

After 500 h of oxidation in air, the sum of all mass gain contributions is in very good agreement with the measured mass gain. Figure 9 shows that the addition of alloying elements decreases the oxide scale thickness, and the decrease in oxide thickness is one of the most significant quantity for the total mass gain.

Optasanu et al. identified a strong correlation between the decrease in total mass gain and the nitrogen uptake, measured by nuclear reaction analysis (NRA), for several modified Ti6242S alloys oxidized at 650 °C for 3000 h [50]. In our study, with similar but also different kinds of alloys, we specify the nature of the correlation. Based on our results, it is not a correlation between the mass gain and the total quantity of N uptake in the system, but a correlation between the oxygen uptake in the metal and the morphology of the nitride layer formed under the oxide scale. Indeed, comparing the Ti_2N surface coverage and the O dissolution in the alloy, it is seen that when the nitride layer is fully covering, as for Ti-(Al)-W alloys, the amount of dissolved O is significantly reduced. A completely covering nitride layer acts as a diffusion barrier for oxygen. If the nitride layer is not continuous, the diffusion barrier is not effective. These results are partly in contradiction with the correlation identified in [50].

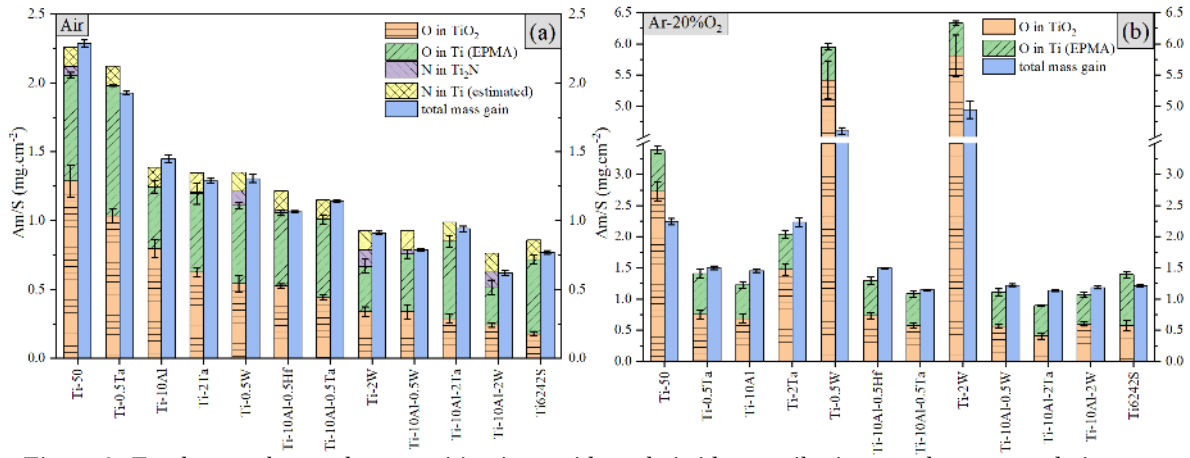

Figure 9: Total mass change decomposition into oxide and nitride contributions, and oxygen and nitrogen diffusion contributions, after 500 h in air (a) and in Ar-20%O_2 (b).

Indeed, pure titanium has the highest mass gain despite forming a nitride layer, while Ti6242S has a very low mass gain, and forms little or no nitride.

In Ar-20%O_2, the decomposition of the total mass gain into O in oxide and O dissolved in the alloy is in rather good agreement with the total mass gain, except for some alloys as Ti-W or pure titanium, where the O mass in the oxide layer seems to be overestimated. There are two main reasons which can explain this overestimation. The first one is an underestimation of the void fraction in the oxide scale, which leads to an overestimation of the mass gain of O in the oxide scale. The second reason is mass loss due to W volatilization. Indeed, several tungsten oxide species were identified to be volatile above 650 °C [51]. To evaluate this possibility, EDS measurements (not shown here) were performed in Ti-2W alloy oxidized under Ar-20%O_2. A slightly lower concentration of W was measured in the oxide scale than in the alloy. If this were due to volatilization, it would correspond to a loss of 15% of the total amount of W in the oxide scale. This corresponds to a mass loss of about 0.13 mg.cm^{-2}, which is much lower than the differences of mass gains visible in Figure 9. This suggests that W volatilization cannot be the only explanation of the difference between the measured mass gain and the calculated mass gain in Fig. 9.

The decomposition of the total mass gain highlights the effect of refractory elements on the decrease in the mass gain due to the oxide thickness, as shown previously in Table 3. The effect of alloying refractory elements on the parabolic constant k_p is mostly due to the decrease of the oxide growth component k_p^{oxide} of the overall parabolic constant rather than the oxygen dissolution component k_p^{diss}, except for W-containing alloys which also reduce k_p^{diss} by the decrease of the oxygen concentration at the nitride/alloy interface.

Aluminium reduces the O diffusivity, tungsten decreases the O concentration at the surface and both of these effects reduce the O dissolution. Ternary Ti-10Al-W alloys combine these two effects and thus Al and W are promising elements for the decrease of the O uptake and alloy embrittlement.

Effect of tungsten on nitride formation

As shown above, the decrease in the oxygen concentration at the nitride/metal interface of the W-containing alloys oxidized in air is correlated with the presence of the nitride layer just below the oxide scale. The nitride layer plays the role of an oxygen diffusion barrier, reducing the O inflow in the alloy [36, 42]. Previous studies have focused on the effect of nitrogen on oxidation kinetics. In particular, it has been shown previously that the presence of nitrogen in the oxidation environment decreases the oxidation kinetics of Ti-based alloys [13, 19, 30, 33, 52], and that a nitridation treatment before oxidation also reduce the mass gain of Ti alloys [53]. Chaze and Coddet showed that the oxygen dissolution was lowered for oxidation treatments in air compared to pure oxygen, and chromium

or titanium nitrides (Cr_2N or TiN) were identified at the metal-oxide interface for Ti-Cr and Ti-Si binary alloys [30]. Vojtěch et al. revealed the presence of titanium nitride TiN in binary Ti-Si alloys with very high Si content (2 and 8 wt. %) [10]. Göbel et al. studied a Ti-4wt%Nb binary alloy and showed the presence of a Ti_2N nitride layer below the oxide scale, associated with a large decrease of the oxidation kinetics and of O dissolution in the alloy [13].

We have shown in the present work that the decrease in the oxygen dissolution in the alloy is due to an indirect effect of W. Indeed, W favors titanium nitrides formation below the oxide scale. During oxidation in Ar-20%O_2, W even has a negative effect on the oxide scale growth. On the contrary, other alloying elements such as Ta and Al seem to destabilize titanium nitrides. In the case of Ti-10Al alloy, no nitride was observed either in this study or in previous studies [8]. From this study and previous observations made on the literature, it can be concluded that there is a group of alloying elements (Nb, Si and W) that promote nitride formation, even if the cause of this effect is not explained yet. Here, it is worth recalling that the presence of nitrogen in solution in α-Ti, up to 20 at. %, limits the O concentration to 1 at. % below the nitride scale [36]. This could be sufficient to form an oxygen diffusion barrier, as proposed by Chaze and Coddet [30]. However, due to the observed correlation between higher coverage of the nitride layer and reduced oxygen uptake, this study indicates that the formation of a continuous Ti_2N nitride layer is a more efficient mechanism for minimizing oxygen ingress.

The enhanced of the nitride formation could be due to a thermodynamic reason, such as the stabilization of the nitride phase by a decrease of nitrogen solubility in the α-Ti phase. It could be due also to kinetic reasons. Nitride precipitation in pure titanium is related to the nitrogen uptake, and in particular linked to the ratio between nitrogen diffusion in the oxide and in the alloy, leading to an accumulation of nitrogen below the oxide scale. Adding refractory elements decrease the oxide thicknesses in air. Since N diffusion in the oxide is controlled by its chemical potential gradient in the oxide, a thinner oxide scale increases the chemical potential gradient in the oxide and thus should increase the nitrogen uptake.

Conclusion

Ti-based model alloys were oxidized at 650°C up to 5000 h in air and for 500 h in Ar-20%O_2 environments, in order to investigate the effect of Al and refractory elements (Hf, Ta and W) on oxidation kinetics and oxygen diffusivities. It was shown that W is the most efficient element in decreasing oxidation kinetics in air, while Ta and Hf have a lesser effect on the oxidation rate. The decrease in the oxidation rate in air is associated with a decrease in the oxide scale growth rate for all alloying elements. The oxygen profiles showed that the presence of

W, Ta or Hf slightly increases the oxygen diffusivity in the α phase (less than a factor of 2), while Al decreases the O diffusivity by a factor of 3 compared to pure titanium. Nevertheless, the presence of W slows down the oxygen dissolution in the alloy due to a significant decrease in the oxygen concentration at the alloy surface. We showed that this is due to the presence of a continuous titanium nitride Ti_2N layer below the oxide scale. The presence of this nitride layer is promoted by some alloying elements, especially by tungsten. Ti-10Al-2W combines the beneficial effects of Al (decreasing the oxygen diffusion coefficient) and W (decreasing the oxygen concentration at the nitride/metal interface where nitride formation is favored), and outperforms Ti6242S in air at 650 °C. Further work will focus on finer analysis of the oxidation products in order to determine the oxygen and nitrogen concentration at the oxide-nitride and nitride-alloy interfaces, but also to understand why W promotes nitride formation.

Acknowledgements

This work was funded in part by the French Government (Direction Générale de l'Aviation Civile) as part of France Relance and Next Generation EU.

The authors gratefully acknowledge Cédric Lopez and Etienne Rimpot (ONERA-DMAS) and Sophie Gouy (UMS Castaing) for alloy elaboration with arc-melting furnace, chemical analysis and EPMA measurements, respectively.

References

[1] M. Peters, J. Kumpfert, C.H. Ward, C. Leyens, Titanium Alloys for Aerospace Applications, Advanced Engineering Materials, 5 (2003) 419-427.
[2] C. Leyens, Oxidation and Protection of Titanium Alloys and Titanium Aluminides, in: Titanium and Titanium Alloys, 2003, pp. 187-230.
[3] R.R. Boyer, Titanium for aerospace: Rationale and applications, Advanced Performance Materials, 2 (1995) 349-368.
[4] H. Okamoto, O-Ti (Oxygen-Titanium), Journal of Phase Equilibria and Diffusion, 32 (2011) 473.
[5] N. Vaché, Y. Cadoret, B. Dod, D. Monceau, Modeling the oxidation kinetics of titanium alloys: Review, method and application to Ti-64 and Ti-6242s alloys, Corrosion Science, 178 (2021) 109041.
[6] A. Casadebaigt, J. Hugues, D. Monceau, High temperature oxidation and embrittlement at 500-600°C of Ti-6Al-4V alloy fabricated by Laser and Electron Beam Melting, Corrosion Science, 175 (2020) 108875.
[7] R.N. Shenoy, J. Unnam, R.K. Clark, Oxidation and Embrittlement of Ti-6Al-2Sn-4Zr-2Mo Alloy, Oxidation of Metals, 26 (1986) 105-124.
[8] A.M. Chaze, C. Coddet, Influence of aluminium on the oxidation of titanium between 550 and 750°C, Journal of the Less-Common Metals, 157 (1990) 55-70.
[9] A.M. Chaze, C. Coddet, G. Béranger, Influence de l'aluminium sur la tenue à l'oxydation du titane entre 550 et 750°C, Journal of the Less Common Metals, 83 (1982) 49-70.
[10] D. Vojtěch, B. Bártová, T. Kubatík, High temperature oxidation of titanium–silicon alloys, Materials Science and Engineering: A, 361 (2003) 50-57.
[11] A.M. Chaze, C. Coddet, Influence of Silicon on the Oxidation of Titanium between 550-Degrees-C and 700-Degrees-C, Oxidation of Metals, 27 (1987) 1-20.
[12] T.C. Valenza, P. Chao, P.K. Weber, O.K. Neill, E.A. Marquis, Protective role of silicon in the high-temperature oxidation of titanium, Corrosion Science, 217 (2023) 111110.

[13] M. Gobel, V.A.C. Haanappel, M.F. Stroosnijder, On the determination of diffusion coefficients of oxygen in one-phase Ti (alpha-Ti) and two-phase Ti-4Nb (alpha- and beta-Ti) by micro-hardness measurements, Oxidation of Metals, 55 (2001) 137-151.
[14] P. Pérez, V.A.C. Haanappel, M.F. Stroosnijder, The Effect of Niobium on the Oxidation Behavior of Titanium in Ar/20% O2 Atmospheres, Oxidation of Metals, 53 (2000) 481-506.
[15] K. Ramoul, C. Coddet, G. Béranger, F. Armanet, Influence des éléments Va sur la résistance à l'oxydation du titane entre 500 et 850°C - I: Cas du vanadium, Journal of the Less Common Metals, 98 (1984) 221-243.
[16] T. Kitashima, Y. Yamabe-Mitarai, S. Iwasaki, S. Kuroda, Effects of Ga and Sn Additions on the Creep Strength and Oxidation Resistance of Near-α Ti Alloys, Metallurgical and Materials Transactions A, 47 (2016) 6394-6403.
[17] Z. Huvelin, C. Gouroglian, N. Horezan, S. Naka, Role of refractory elements in near-alpha titanium alloys on high temperature mechanical properties, in: Titanium 2019, NANTES, France, 2019.
[18] R.J. Hanrahan, D.P. Butt, Oxidation kinetics and mechanisms of Ti-Ta alloys, Oxidation of Metals, 47 (1997) 317-353.
[19] R.J. Hanrahan, D.P. Butt, The effects of nitrogen on the kinetics and mechanisms of oxidation of Titanium-Tantalum alloys, Oxidation of Metals, 48 (1997) 41-58.
[20] R.J. Hanrahan, Jr., Y.C. Lu, H. Kung, D.P. Butt, A study of nitride formation during the oxidation of titanium-tantalum alloys, in, United States, 1996, pp. 14.
[21] Y. Xu, Y. Fu, J. Li, W. Xiao, X. Zhao, C. Ma, Effects of tungsten addition on the microstructural stability and properties of Ti-6.5Al-2Sn-4Hf-2Nb-based high temperature titanium alloys, Journal of Materials Science & Technology, 93 (2021) 147-156.
[22] T. Kitashima, Y. Yamabe-Mtarai, S. Iwasaki, S. Kuroda, Effects of Alloying Elements on the Tensile and Oxidation Properties of Alpha And Near-Alpha Ti Alloys, in: Proceedings of the 13th World Conference on Titanium, 2016, pp. 479-483.
[23] H.W. MAYNOR, JR., R.E. SWIFT, The Scaling of Titanium and Titanium-Base Alloys in Air, Corrosion, 12 (1956) 49-60.
[24] A. Casadebaigt, Etude de l'oxydation à chaud d'échantillons en alliage TA6V élaborés par fabrication additive. Conséquences sur les propriétés mécaniques, in: Thesis, Toulouse University, 2020.
[25] A. Vande Put, C. Dupressoire, C. Thouron, P. Emile, R. Peraldi, B. Dod, D. Monceau, High-Temperature Oxidation Behavior of Ti6242S Ti-based Alloy, Oxidation of Metals, 96 (2021) 373-384.
[26] C. Dupressoire, Oxydation à haute température longue durée de trois alliages industriels à base de titane : effets de la microstructure, de l'environnement (azote et vapeur d'eau) et du cyclage thermique, in: Thesis, Toulouse University, 2018.
[27] J.O. Andersson, T. Helander, L. Höglund, P. Shi, B. Sundman, Thermo-Calc & DICTRA, computational tools for materials science, Calphad, 26 (2002) 273-312.
[28] D. Monceau, B. Pieraggi, Determination of Parabolic Rate Constants from a Local Analysis of Mass-Gain Curves, Oxidation of Metals, 50 (1998) 477-493.
[29] P. Kofstad, High Temperature Oxidation of Metals, Wiley, New York, 1966.
[30] A.M. Chaze, C. Coddet, The role of nitrogen in the oxidation behaviour of titanium and some binary alloys, Journal of the Less Common Metals, 124 (1986) 73-84.
[31] B. Vincent, V. Optasanu, F. Herbst, S. Chevalier, I. Popa, T. Montesin, L. Lavisse, Comparison Between the Oxidation Behaviors of Ti6242S, Ti6246, TiXT Alloys, and Pure Titanium, Oxidation of Metals, 96 (2021) 283-294.
[32] S. Frangini, A. Mignone, F. de Riccardis, Various aspects of the air oxidation behaviour of a Ti6Al4V alloy at temperatures in the range 600–700 °C, Journal of Materials Science, 29 (1994) 714-720.
[33] C. Dupressoire, A. Rouaix - Vande Put, P. Emile, C. Archambeau-Mirguet, R. Peraldi, D. Monceau, Effect of nitrogen on the kinetics of oxide scale growth and of oxygen dissolution in the Ti6242S titanium-based alloy, Oxidation of Metals, vol. 87 (2017) pp. 343-353.
[34] M. Berthaud, Étude du comportement de l'alliage de titane Ti6242S à haute température sous atmosphères complexes : applications aéronautiques, in, 2018.
[35] K. Wiedemann, R. Shenoy, J. Unnam, Microhardness and lattice parameter calibrations of the oxygen solid solutions of unalloyed α-titanium and Ti-6Al-2Sn-4Zr-2Mo, Metallurgical Transactions A, 18 (1987) 1503-1510.
[36] C. Dupressoire, M. Descoins, A. Vande Put, E. Epifano, D. Mangelinck, P. Emile, D. Monceau, The role of nitrogen in the oxidation behaviour of a Ti6242S alloy: a nanoscale investigation by atom probe tomography, Acta Materialia, 216 (2021) 117134.
[37] S.H. Cheung, P. Nachimuthu, A.G. Joly, M.H. Engelhard, M.K. Bowman, S.A. Chambers, N incorporation and electronic structure in N-doped TiO2(110) rutile, Surface Science, 601 (2007) 1754-1762.
[38] J. Stringer, The oxidation of titanium in oxygen at high temperatures, Acta Metallurgica, 8 (1960) 758-766.
[39] J. Crank, The mathematics of diffusion, Second edition ed., Clarendon Press, Oxford, 1975.
[40] Thermo-Calc Software, MOBTI3: Ti-alloys Mobility Databse, in.

[41] D. David, G. Beranger, E.A. Garcia, A study of the diffusion of oxygen in alpha-titanium oxidized in the temperature range 460°-700°C, J. Electrochem. Soc., 130 (1983) 1423-1426.
[42] V. Optasanu, P. Berger, M.C. Marco de Lucas, M.K. Rayhan, F. Herbst, N. Geoffroy, O. Heintz, I. Bezverkhyy, S. Chevalier, T. Montesin, L. Lavisse, Nitrogen quantification and tracking during high temperature oxidation in air of titanium using 15N isotopic labelling, Corrosion Science, 216 (2023) 111072.
[43] M. Raffy, Etude de l'oxydation de l'alliage eutectique Ti-Si à 8,5% en poids de Si aux températures inférieures à 850°C. Influence de l'état structural, in, Ecole Nationale Supérieure de Chimie de Paris, 1981.
[44] K.N. Strafford, A comparison of the high temperature nitridation and oxidation behaviour of metals, Corrosion Science, 19 (1979) 49-62.
[45] F.L. Bregolin, M. Behar, F. Dyment, Diffusion study of 15N implanted into α-Ti using the nuclear resonance technique, Applied Physics A, 90 (2008) 347-349.
[46] F.L. Bregolin, M. Behar, F. Dyment, Diffusion study of 18O implanted into α-Ti using the nuclear resonance technique, Applied Physics A, 86 (2007) 481-484.
[47] J.C. Schuster, J. Bauer, The ternary system titanium-aluminum-nitrogen, Journal of Solid State Chemistry, 53 (1984) 260-265.
[48] A. Anttila, J. Räisänen, J. Keinonen, Diffusion of nitrogen in α-Ti, Applied Physics Letters, 42 (1983) 498-500.
[49] H.R. Ogden, R.I. Jaffee, THE EFFECTS OF CARBON, OXYGEN, AND NITROGEN ON THE MECHANICAL PROPERTIES OF TITANIUM AND TITANIUM ALLOYS, in, United States, 1955, pp. Medium: ED; Size: Pages: 99.
[50] V. Optasanu, P. Berger, B. Vincent, M.C. Marco de Lucas, F. Herbst, T. Montesin, L. Lavisse, Strong correlation between high temperature oxidation resistance and nitrogen mass gain during near alpha titanium alloys exposure in air, Corrosion Science, 224 (2023) 111547.
[51] G.A. Greene, C.C. Finfrock, Vaporization of tungsten in flowing steam at high temperatures, Experimental Thermal and Fluid Science, 25 (2001) 87-99.
[52] I. Abdallah, C. Dupressoire, L. Laffont, D. Monceau, A. Vande Put, STEM-EELS identification of TiOXNY, TiN, Ti2N and O, N dissolution in the Ti2642S alloy oxidized in synthetic air at 650 °C, Corrosion Science, 153 (2019) 191-199.
[53] P. Pérez, Influence of nitriding on the oxidation behaviour of titanium alloys at 700 °C, Surface and Coatings Technology, 191 (2005) 293-302.